Report no. changed (Mar 2006): SM-346-UU

NATO OTAN

Undersea Research Centre
Centre de Recherche Sous-Marine

The application of parametric side scan sonar to the detection of proud and buried targets

E. Bovio
A. Maguer
S. Fioravanti

NORTH ATLANTIC TREATY ORGANISATION ORGANIZATION DU TRAITE DE L'ATLANTIQUE NORD

January 1998 Report SM-346

Report no. changed (Mar 2006): SM-346-UU

SACLANTCEN SM-346

The application of parametric side scan sonar to the detection of proud and buried targets

E. Bovio, A. Maguer, S. Fioravanti

The content of this document pertains to work performed under Project 031-1 of the SACLANTCEN Programme of Work. The document has been approved for release by The Director, SACLANTCEN.

Jan L. Spoelstra
Director

intentionally blank page

SACLANTCEN SM-346

The application of parametric side scan sonar to the detection of proud and buried targets

E. Bovio, A. Maguer, S. Fioravanti

Executive Summary: Mines are usually detected by high-frequency, sonar imaging systems which, due to absorption of high-frequency sound by bottom sediment, are severely limited in effectively detecting buried targets. This report describes the use of side scan parametric sonar (secondary frequency 2**-**12 kHz and primary frequency 40 kHz) at very low grazing angles for the detection of mines. The advantages of this technique are the deep penetration into the sediment of the secondary frequency waves, the high directivity (reduced bottom reverberation) of the parametric sonar and the potentially large area covered by the low grazing angle insonification.

Detection ranges achieved for the dual frequency parametric sonar, were measured using cylindrical dummy targets and exercise mines, positioned proud on the bottom, with unknown orientation. Detection ranges of 750 m were achieved with the low frequency parametric sonar. Detection performance against buried targets has been extrapolated by means of a simple model based on Lambert's law.

It is shown that the technique is unlikely to detect a –18 dB target buried in sand, if the transmission loss due to sediment penetration exceeds 2 dB (one way propagation). Detection performance would be improved with the use of a 128 element receiving array, which would allow detection of the same target buried in sediment, with one way transmission loss of the order of 6 or 7 dB.

In order to better characterize the performance of a low grazing angle sonar against buried targets, it is important to understand the propagation loss of the transmitted pulses into the sediment. For this reason, a few experiments have already been planned to measure the frequency response of the sediment as a function of bottom type, transmitted frequency, burial depth and grazing angle. At the same time, the spatial response of the buried targets will be studied, with models and field experiments, over a broad range of frequencies, burial depths and grazing angles.

Future work will include the evaluation at sea of the side scan parametric sonar approach, combined with the new 128 element array for the detection of buried targets. Different ranges (i.e. different grazing angles) from the sonar to the targets will be considered, in order to evaluate the performance of the selected approach for the detection of buried mines, as a function of grazing angles.

intentionally blank page

SACLANTCEN SM-346

The application of parametric side scan sonar to the detection of proud and buried targets

E. Bovio, A. Maguer, S. Fioravanti

Abstract: This paper describes an experiment designed to evaluate the feasibility of using the TOPAS parametric transmitter mounted in side scan mode, for the detection of buried targets. The concept was tested with proud targets in order to evaluate the detection ranges achieved for low and high frequencies of the parametric sonar. The performance against buried targets has been estimated by means of a simple model based on Lambert's law.

Detection of a variety of cylindrical proud targets on a sandy bottom has been achieved in reverberation and noise limited conditions up to a range of 750 m, using both the primary (40 kHz) and secondary frequencies (2 to 12 kHz) of the parametric source.

In reverberation, short, broadband, Ricker pulses were used to improve the range resolution of the sonar, while at longer range 10 ms LFM pulses were transmitted to counter the noise level. The secondary frequency of the TOPAS achieved better results : the LF mode of operation achieved 30 detections against a mine field of six different targets and 10 detections against a cluster of three targets. The HF mode had only 15 detections against the mine field, and 10 detections against the cluster. Comparing the Signal to Background Ratio (SBR) for all targets detected by both HF and LF, the LF outperforms the HF. Although the TS of the targets should theoretically increase from LF to HF, the SBR is in average about 2 dB higher at low frequency.

The conditions of the experiment were modelled with a simple sonar equation based on Lambert's law. There is good agreement between modelled and measured target echo levels. Measured reverberation is higher than that predicted by Lambert's law. A parametric study was performed to assess the amount of extra loss that the sonar could afford, when the transmitted pulses propagate into the sediment. The proposed sonar was unlikely to detect a target of –18 dB buried in sand, if the extra transmission loss into the sediment exceeds 2 dB (one way propagation). This negative result can be partly overcome by a longer receiver to improve horizontal resolution. The effect of an 128 element array has also been modelled and the upgraded sonar should be capable of achieving detections of a –18 dB target buried in sand, with one way transmission loss of the order of 6 or 7 dB.

Keywords: TOPAS – proud target detection – Lambert's law

Contents

1 Introduction

The problem of detecting and classifying buried mines is of critical importance to NATO. Mines are usually detected by high-frequency imaging sonar systems which, due to absorption of high-frequency sound by bottom sediment, are severely limited in effectively detecting buried targets.

SACLANTCEN has investigated a number of alternatives including the TOPAS [1] parametric array used as side scan sonar, at very low grazing angles (well beyond the critical angle). The main advantages of parametric sonar are the generation of low-frequency waves (which penetrate more deeply into the sediment), high directivity (that of the primary high frequency) without side lobes (less bottom reverberation) and wide bandwidth. The main limitation of parametric sonar, is poor efficiency at low frequency. A major advantage of the low grazing angle option in shallow water, is large area coverage, compared to traditional systems using normal incidence or swath survey approaches. The low grazing angle option pursued by the Centre, is however very challenging, given that according to reflection theory, there is no penetration into sediment and thus no detection of buried objects should be possible, while operating below the critical angle.

There is however substantial evidence of penetration below the critical grazing angle, which justifies the selected approach. At present, four mechanisms have been hypothesized, the porous nature of the sediment which leads to a second “slow” compressional wave with a wave speed less than the speed of sound in water [2], the roughness of the water-sediment interface [3], the effect of using a narrow beamwidth [4] and volume inhomogeneities within the sediment which scatter the evanescent wave [5]. It has been observed that the level of energy penetrating sediment at below critical angle is higher than predicted by evanescent theory [6].

The aim of this paper is to describe the first experiment, which was designed to evaluate the feasibility, and potential of the selected concept for the detection of buried targets. The selected concept was tested with proud targets in order to evaluate the detection ranges achieved for the primary and secondary frequencies of the parametric sonar. The targets were cylinders positioned on the bottom with unknown orientation. The TS of the targets was therefore unknown given the extreme variation with aspect angle of cylinder TS.

Section 2 describes the experimental configuration. The characteristics of the parametric sonar TOPAS are given including transmitting and receiving directivities, and the transmitted signals that were either Ricker signals or linear frequency modulated (LFM) signals. The receiving directivity of a rigid 16 hydrophone array, which was combined

with the parametric sonar in order to increase the receiving directivity of the parametric sonar, is also given.

Section 3 describes the results obtained in reverberation-limited conditions (closer ranges) and noise-limited conditions (longer ranges). In reverberation-limited conditions it was found that the echo-to-reverberation ratios were of the order of 10 to 20 dB for the different targets. Better detection was achieved at low frequencies. In noise-limited conditions, LFM signals were transmitted and a matched filtering technique was applied. Detection ranges of approximately 750 m were achieved against proud targets with the low frequency of the parametric sonar.

Section 4 is dedicated to sonar equations. Comparison of the detection ranges obtained during the experiment with the detection ranges predicted by basic sonar equations is performed. The measured reverberation and target echo levels are compared with the values predicted by the models. To evaluate the maximum permissible loss into sediment, a parametric analysis is performed for a 16 element receiving array and for a 128 element array.

2 Experimental configuration

To demonstrate the feasibility of the concept, an initial experiment was designed to evaluate detection ranges in shallow water against proud targets.

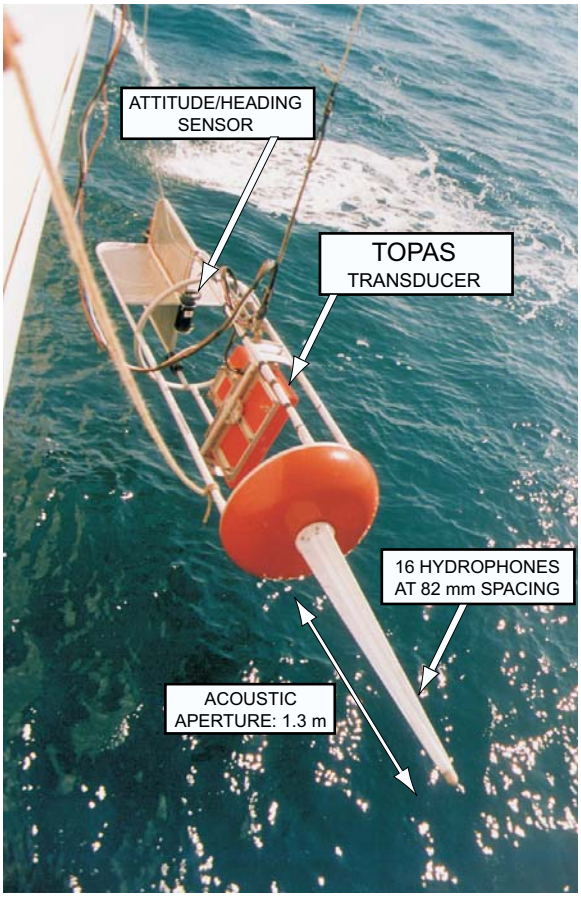

Figure 1: Experimental configuration showing the TOPAS transmitter, the 16-element receiving array, and the attitude and heading sensors

Figure 1 shows the TOPAS array mounted in Side Scan Sonar (SSS) mode and the receiving array of 16 hydrophones. The unit was towed alongside NRV *Alliance* at a depth below the surface of 2.5 m over a sandy bottom in 26 m, over a target field of metal cylinders filled with concrete and exercise mines.

SSS is a real beam imaging technique that provides two dimensional reflectance images of acoustic backscatter energy from targets positioned on the ocean floor or buried in sediment. SSS systems insonify narrow sections of sea floor using an acoustic projector towed by a platform moving in a straight line with constant velocity V as shown in Figure 2. In this figure, ϕ_E and ϕ_H are the elevation and azimuth beamwidth of the projector, h is the distance of the sonar from the bottom, R is the instantaneous slant range measured from the sonar to a target on the sea floor, and W is the insonified sea floor area. Only the area A, of width $R\phi_H$ and range extension $c\tau/2$ (where c is the sound speed in water and τ is the range resolution of the transmitted signal), returns reverberation at any instant of time. The reflectance image has coordinates of cross-track (measured in the slant plane) and along track distances. As the platform moves, the projector transmits acoustic pulses and an array of hydrophones listens for the echoes: the time delay of each echo provides a measure of the slant range, while the ping-to-ping motion of the projector gives the along track image dimension.

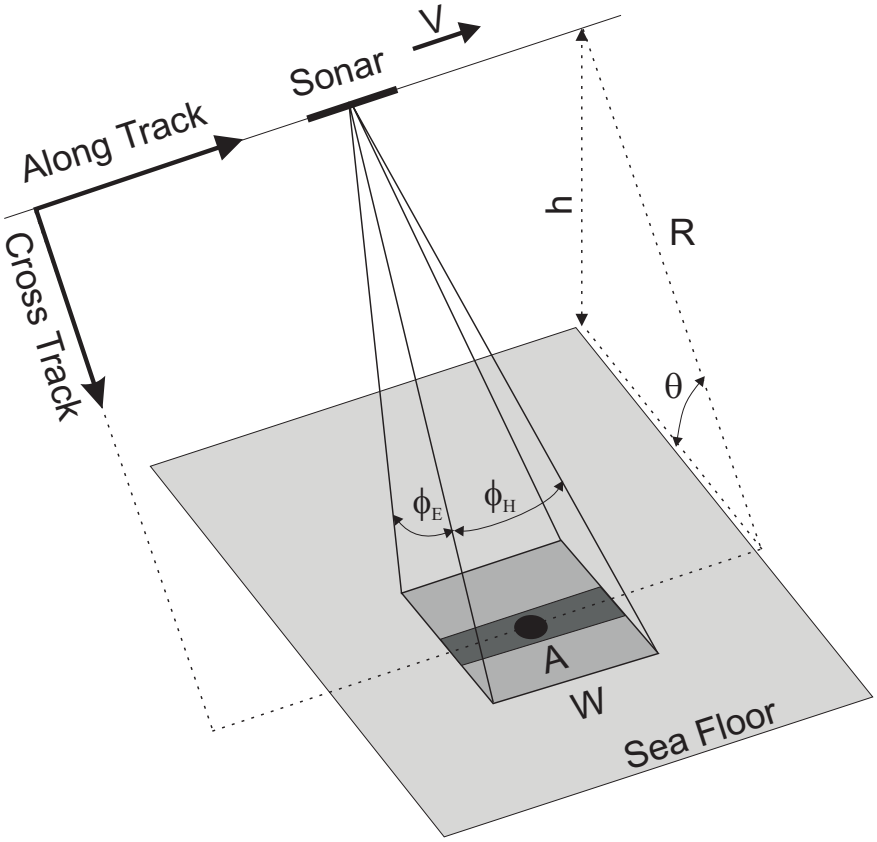

Figure 2 : Geometry of Side Scan Sonar

2.1 The transmitting and receving system

2.1.1 The source

The parametric sonar used was the SIMRAD TOPAS (TOpographic PArametric Sonar). A short single pulse is obtained by transmitting a weighted HF-burst at the primary frequency. The TOPAS transducer consists of 24 staves, electronically controlled to form a beam in a selected direction (~ 40°). The primary frequency is 40 kHz, the difference frequency from 2 kHz to 12 kHz. The transmitting source level is approximately 244 dB for the primary frequency. The source levels obtained at different frequencies vary from about 190 to 213 dB/1 µ Pa ref. 1 m using frequency from 2 to 12 kHz.

To detect the targets, Ricker pulses and LFMs of various bandwidth and duration were transmitted centered around the primary and secondary frequencies of the parametric sonar

Figures 3 and 4 show Ricker and LFM pulses and their spectra at secondary frequency.

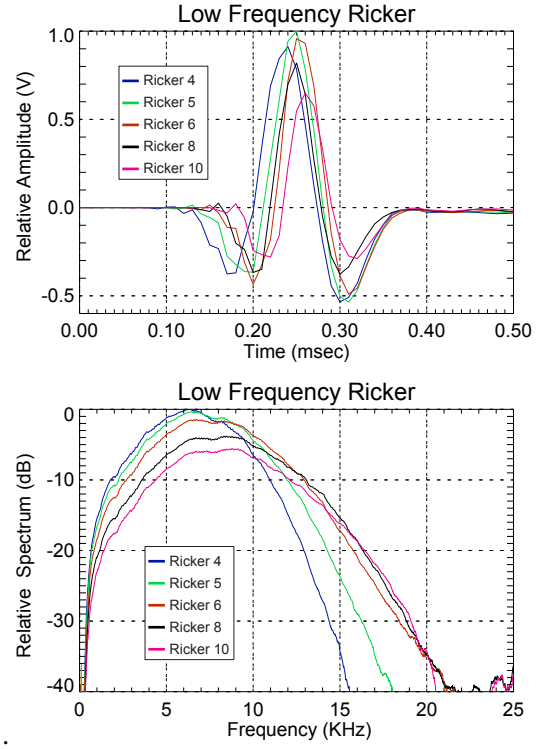

Figure 3 : Ricker pulses and their spectra at secondary frequency

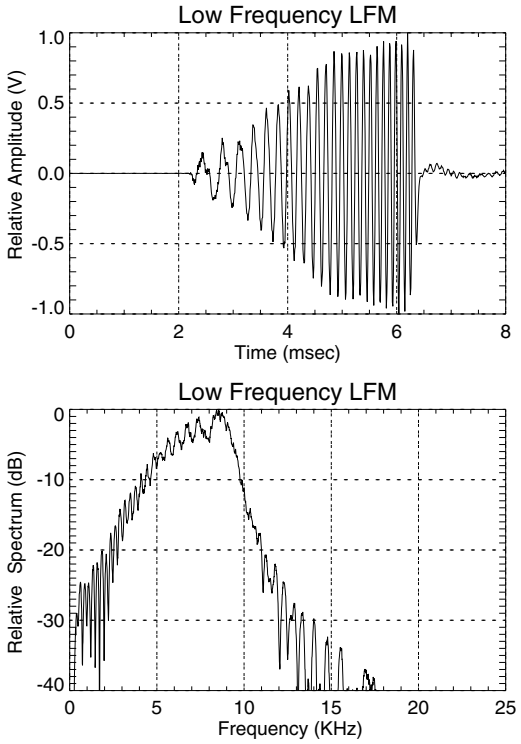

Figure 4 : LFM pulse and its spectrum at secondary frequency

The beam pattern of the difference frequency has good directivity (similar to the high frequency conventional sonar) and extremely low side-lobes as shown in Figure 5a, and 5b.

2.1.2 The receiver

The receiving array consists of 16 hydrophones with 82 mm spacing which generate a total acoustic aperture of 1.3 m. The receiving beam pattern is displayed in Figure 5c.

The low frequency (LF) signals received by the hydrophones array were summed to form a broadside beam, and processed for replica correlation and envelope detection to form the image of the insonified bottom area. The high frequency (HF) signals were received by the directional high frequency receiver of the TOPAS and were processed and displayed in a similar way.

(a)

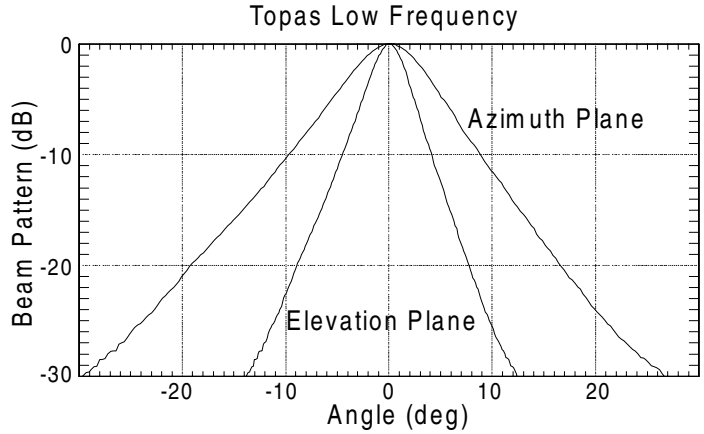

(b)

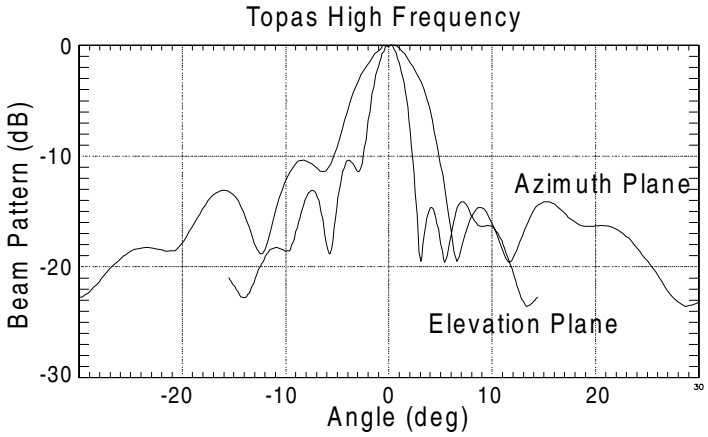

(c)

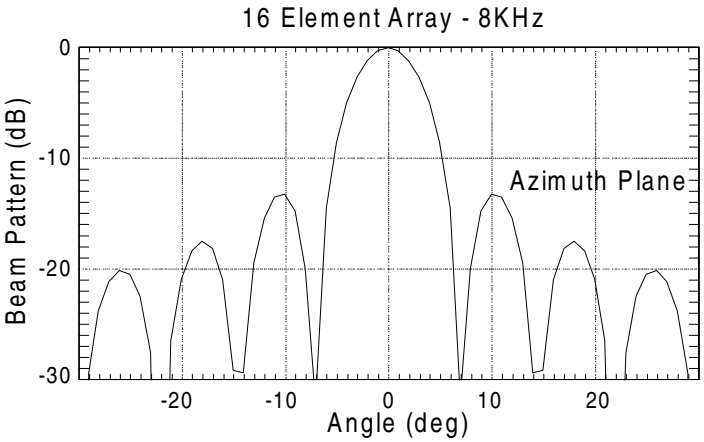

Figure 5 : Transmit (a) (b), and receive beam patterns (c) of the experimental sonar

Figure 6 shows the diagram of the data acquisition system. The hydrophones signals were recorded on two systems: the ADAM and the TOPAS acquisition system. The data from

the array were recorded on the ADAM system, while analog beamformed data for the primary and secondary frequency were stored onto the TOPAS station.

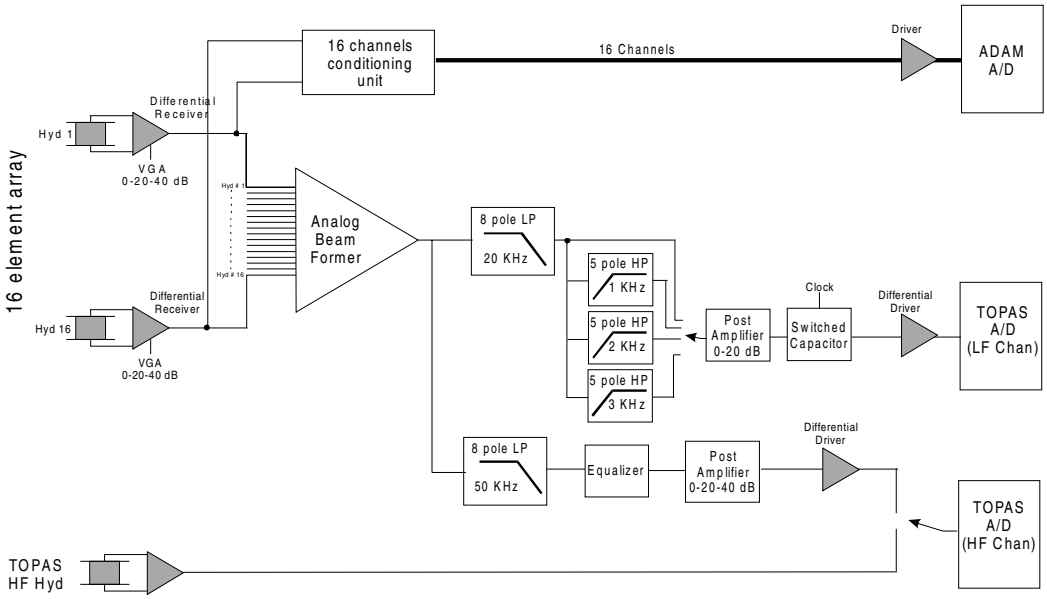

Figure 6 : Block diagram of data acquisition system

The output of the analog beamformer is the unfocused broadside beam of the 16 element array. The sampling rate for the low frequency data was 100 kHz on both systems, while the high frequency channel was sampled at 133 kHz.

Figure 7 shows the noise spectrum measured by the array when the sonar was towed at a speed of 1 kn at 2 m and 4 m depth. The numbering of the hydrophones starts from the tow-body (i.e. channel 0 is the hydrophone closest to the tow body). The high noise measured in the low part of the spectrum is due to mechanical vibration of the array, as the noise level increase with the distance from the tow-body.

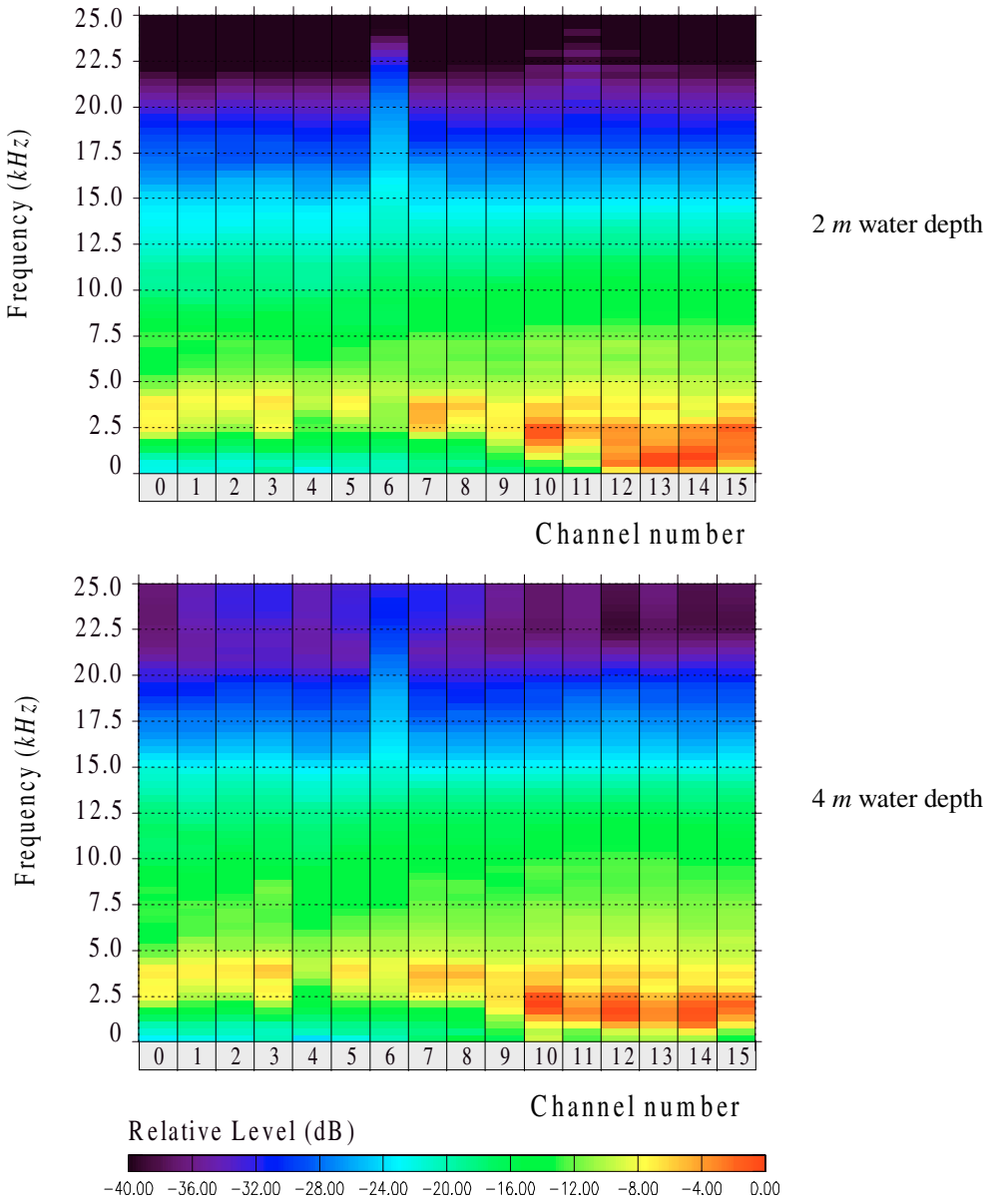

Figure 7 : Noise spectrum measured on the 16-element array showing high levels in the lower part of the spectrum due to mechanical vibrations

In order to process the data, it was necessary to remove this low frequency noise by applying a band pass filter to the signals from 3 to 15 kHz. Figure 8 shows a target echo before and after filtering.

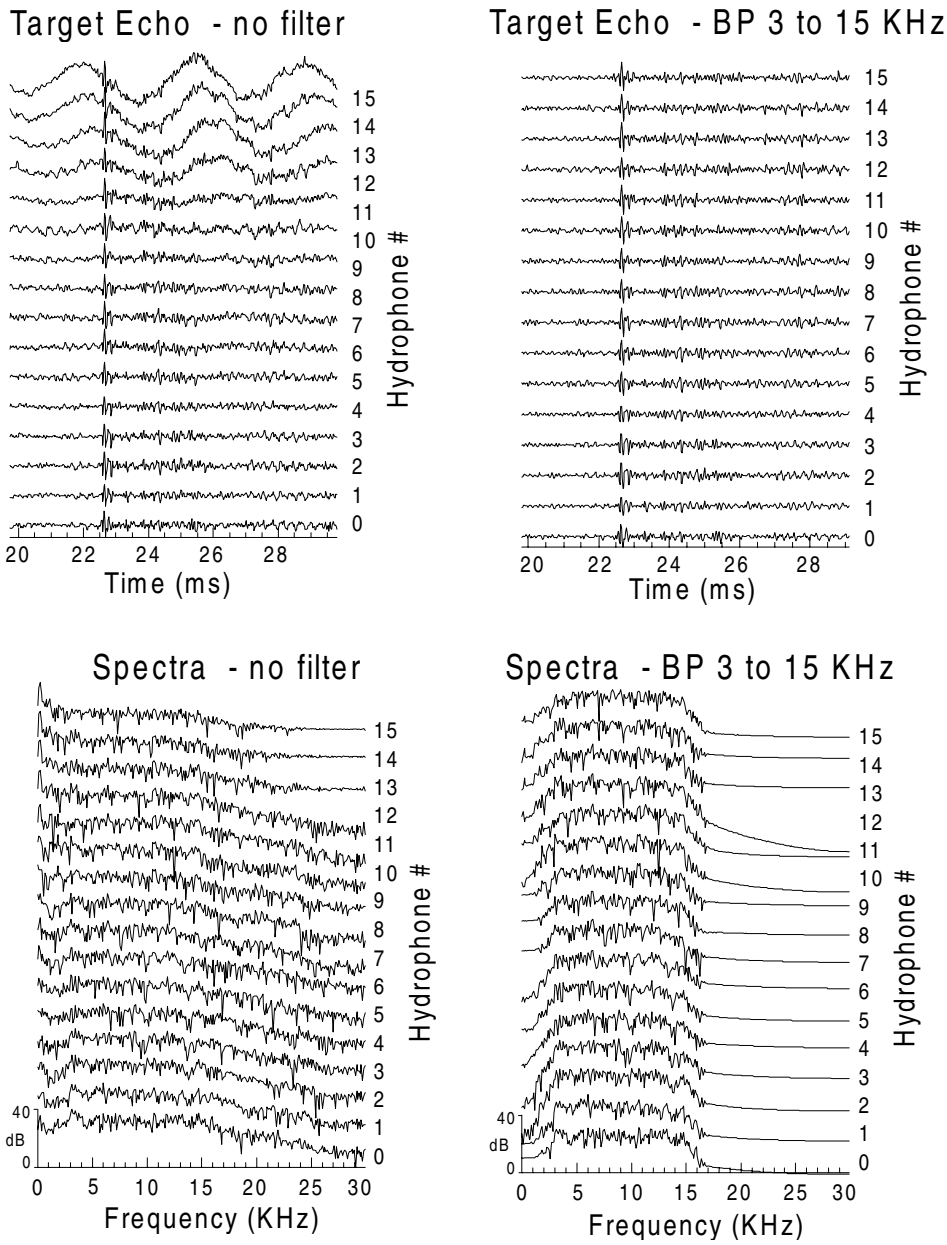

Figure 8 : Target echoes and their spectra measured on the 16 element array before and after bandpass filtering. The filter has removed most of the interference on the high numbered hydrophones due to mechanical vibration of the array

2.2 The towed-fish configuration and motion compensation operations

The TOWPAS structure is a towed frame for the TOPAS parametric sonar (see Figure 9). The frame is intended to carry the TOPAS transducer and also the TOPAS hydrophones in a sub-vertical layout to allow insonification of the searched area with no or minimum interaction with the ship hull. The TOWPAS frame is also fitted with a MRU (Motion Reference Unit) which will measure its heading, roll, pitch and heave. On the bow of this frame a 16 hydrophone linear rigid array is installed.

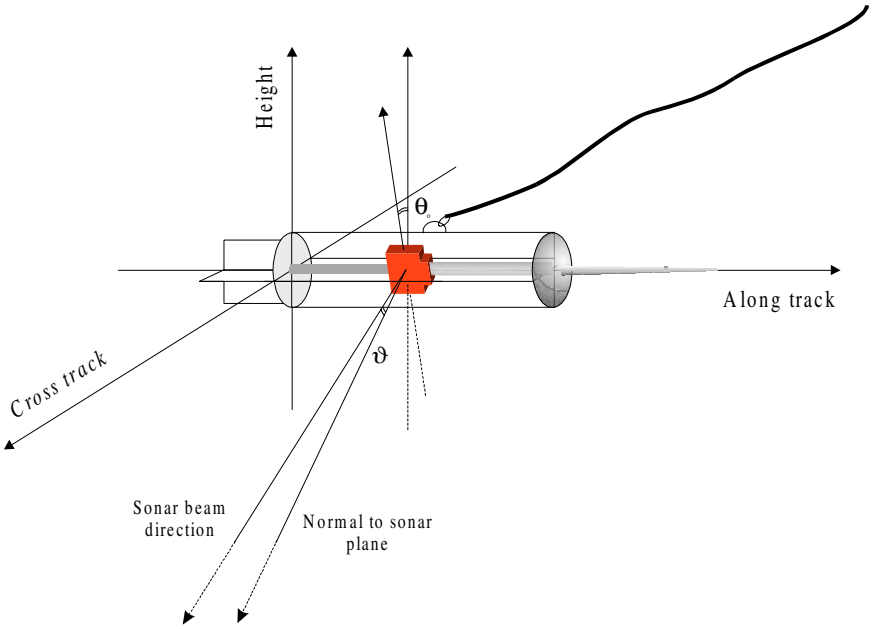

Figure 9 : Geometry of the TOWPAS sonar

The tow-body lengths are 2.7 m and 4.5 m without and with the array respectively. The transducer is mounted in the fish with an inclination θ_0 as shown in Figure 9. The TOPAS has the possibility to steer the beam in the vertical plane of an angle ϑ in the range [-40°, +40°].

The Motion Reference Unit (MRU) can measure the three movements shown in Figure 10 the pitch φ and the roll ρ are angles due to rotations; the heave h is the variation in the vertical direction. During navigation the fish was quite stable in terms of heave and pitch, but roll was significant. For this reason, the automatic roll compensation provided by the TOPAS system was used.

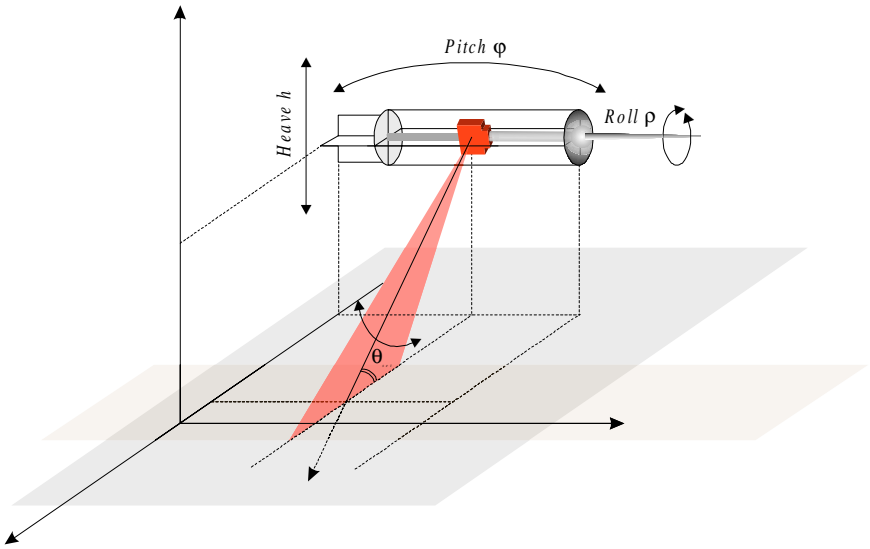

Figure 10 : Motion of the TOWPAS sonar

The sonar uses the MRU data to compute the steering direction $\vartheta = \vartheta_{comp}$ given by:

$$\vartheta_{comp} = \vartheta_{set} - \rho \quad \text{where} \quad \vartheta_{set} = \theta_{set} - \theta_0$$

Therefore, if the sonar operator sets the desired grazing angle to $\theta = \theta_{set}$, the system automatically steers the beam to obtain that grazing angle. Problems can occur when the necessary correction is not in the range [-40°,+40°] but also significant variation of the received signal can be observed when the absolute correction is greater than 10° as, beyond that angle, the sonar source level (*SL*) variation is notable. During the trial roll angles up to 7° were measured.

2.3 Description of targets

The mine field consisted of 6 targets uniformly spaced on the bottom along a straight line. The cluster was composed of the three cylinders Cyl1, Cyl2 and TNO attached together with some ropes. The targets forming the cluster were too close to be resolved in azimuth, but sufficiently separated to be resolved in range. The characteristics of the targets are summarized in Table 1

Targets	Type	Dimensions		ka	kl	ka	kl
		diam. (m)	length (m)	prim. freq	prim. freq	sec. freq	sec. freq
Cyl1	Concrete cylinder	0.5	1.5	42	126	6	19
Cyl2	Concrete cylinder	0.5	1.5	42	126	6	19
TNO	Mild steel shell cylinder	0.5	2	42	167	6	25
IT1	Italian exercise mine	Classified	Classified	Classified	Classified	Classified	Classified
IT2	Italian exercise mine	Classified	Classified	Classified	Classified	Classified	Classified
IT3	Italian exercise mine	Classified	Classified	Classified	Classified	Classified	Classified

Table 1 : Characteristics of targets

2.4 Description of area

The experiment was performed off Viareggio in a sandy area having the following coordinates N434900 N435000 E1003800 E1004200. The water depth was 26 m. The sound speed in the water was 1520 m/s. The sound speed in the bottom obtained from a core is tabulated below:

Depth (cm)	Sound speed (m/s)
2.5	1524
5	1563
10	1688
15	1692
20	1681
25	1714

Table 2 : Summary of sound speed in the bottom in the area of experiment

Figure 11 shows examples of two runs for testing detection performances against mine field and cluster. Many similar runs were conducted with different ship headings.

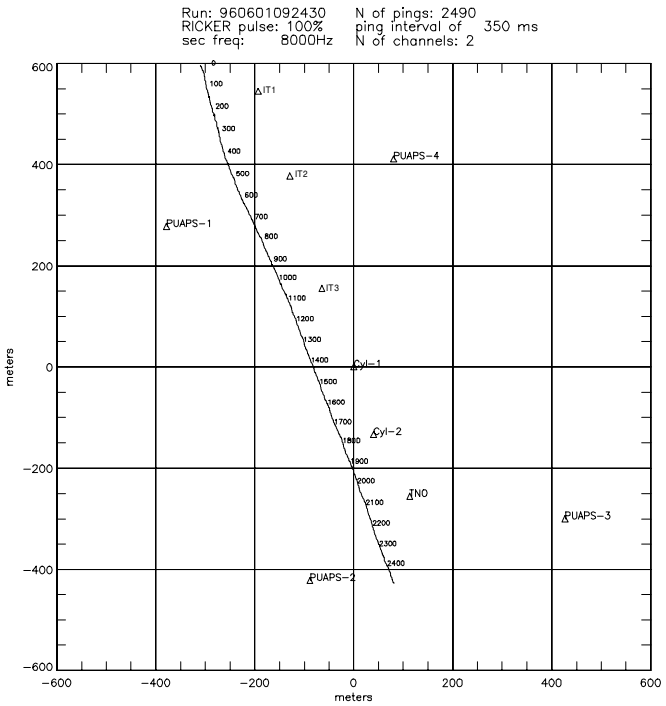

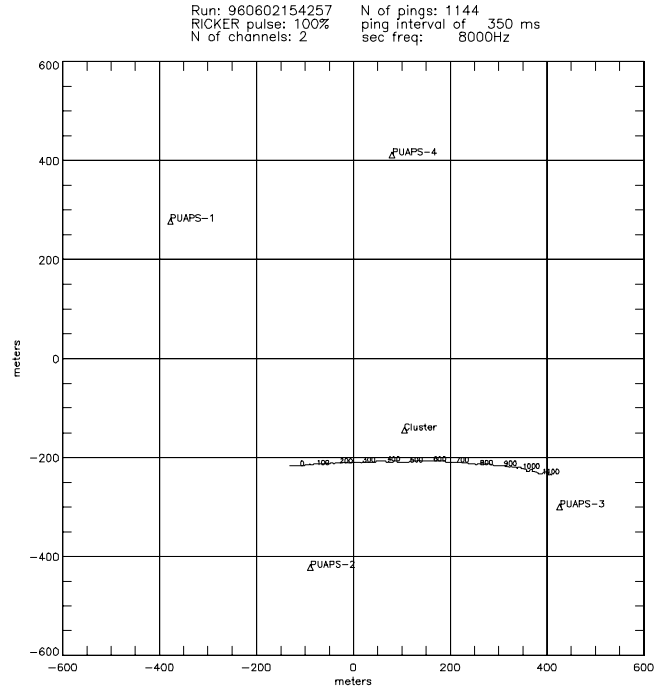

Figure 11: Examples of two runs with mine field and cluster showing ship tacks and mines position

3
Experimental results

This section presents the experimental results and analyzes the signals acquired by the TOPAS receiving chain, and the ADAM system.

In the first case, due to problems in the recording of the gain settings utilized, it was not possible to reconstruct the absolute levels of the received signals, and therefore results are presented in relative terms only. For the ADAM runs, as it was possible to have a complete calibration of the acquisition chain, all results are presented in absolute levels and are also compared with a simple model of the sonar equation.

3.1 Definition of sonar equation parameters

The definitions of the sonar equation parameters used in the report, and the methods used to measure them, are listed below.

3.1.1 Target Range (R)

The Target Range *R* is the minimum slant range measured during a transit from the sonar to a target on the sea floor

3.1.2 Target Grazing Angle (θ)

The Target Grazing Angle θ is the incident angle of the transmitted sonar pulses on the target.

3.1.3 Echo Level (EL)

The Echo Level is the average intensity of the target echo measured at the output of the directional receiving element. For the TOPAS HF runs this is the TOPAS hydrophone; for the TOPAS LF runs this is the analog broadside beam of the 16 element array, and for the ADAM LF runs this is the digital broadside beam of the 16 element array.

As the sonar moves in the water, each target is insonified by multiple pings which generate multiple returns lined up in a parabolic track. To measure the *EL,* the maximum

response of the target has been selected and the returned intensity has been averaged over the pulse duration.

$$EL = -S_h - G + 10\log(\frac{1}{T_1 - T_0}\int_{T_0}^{T_1} v_{tar}^2 dt) \quad (1)$$

Where S_h is the sensitivity of the receiving hydrophones, G is the total gain of the acquisition chain, and v_{tar} is the instantaneous voltage of the target echo at the output of the directional receiving element.

For Ricker pulses, the time window $[T_0, T_1]$ has been selected to contain all energy of the signal: following [7] a duration of .25 ms has been selected, centred around the peak of the maximum response of the target.

For high signal to background ratios (SBR), the instantaneous intensity of the target echo, practically coincides with the total signal measured at the array output, and the contribution of the background (noise or reverberation) can be ignored:

$$Max(v_{tar}^2) \cong Max(v_{tar+bgnd}^2) \quad (2)$$

Consequently, for SBR higher than 10dB, the EL becomes

$$EL = -S_h - G + 10\log(\frac{1}{.25*10^{-3}}\int_{t_{\max}-.125*10^{-3}}^{t_{\max}+.125*10^{-3}} v_{tar+bgnd}^2 dt) \quad (3)$$

Where t_{max} is the time when the maximum response of the target occurs. The maximum is searched over all pings of the target track.

As the transmit beam pattern of the sonar was not in general aligned with the target in the elevation plane, the measured EL is lower than that which would have occurred if the sonar had been pointed directly at the target. In order to compare the measured data with a simple sonar equation, we need to compensate for the beam pattern effects, and define the corrected echo level EL_{cor} as

$$EL_{cor} = EL + BP(\phi_E - \theta) \quad (4)$$

Where ϕ_E is the direction of the transmit beam in the elevation plane and θ is the target grazing angle. $BP(\phi_E-\theta)$ is a correction factor that takes into account that the target does not lie on the main axis of the transmit beam, and is computed by taking the difference in decibels between the value along the main axis of the transmit beam pattern in the elevation plane and the value of the transmit beam pattern in the elevation plane at an angle $(\phi_E-\theta)$ off the main axis.

3.1.4 Transmission Loss (TL)

The one way Transmission Loss *TL* has been approximated by spherical spreading of the transmitted signal computed at the target range *R*. Therefore

$$TL = 20\log(R) \tag{5}$$

3.1.5 Reverberation Level (RL)

To estimate the Reverberation Level *RL*, a similar approach to that of the *EL* has been used: for each run, all pings that do not contain target echoes have been selected, and *RL* has been measured as a function of range *r* as follows

$$RL(r) = -S_h - G + 10\log[\frac{1}{n}\sum_{i=1}^{n}(\frac{1}{.25*10^{-3}}\int_{(2r/c)-.125*10^{-3}}^{(2r/c)+.125*10^{-3}} v_{rev_i}^2 dt)] \tag{6}$$

Where c is the sound speed, n is the number of pings used in the average (typically 100 pings), and v_{rev_i} is the instantaneous voltage of the reverberation for ping i at the output of the directional receiving element. The computation of *RL* has been limited to the range interval where the reverberation was stronger than the noise. As in the case of the *EL*, also *RL* depends on the direction of the transmit beam in the elevation plane. In order to average *RL* over many runs and to compare it with a simple model based on Lambert's law, we correct it for the beam pattern effects

$$RL_{cor}(r) = RL(r) + BP(\phi_E - \theta_r) \tag{7}$$

Where ϕ_E is the direction of the transmit beam in the elevation plane and θ_r is the grazing angle of the incident wave at range *r*.

3.1.6 Noise Level (NL)

The noise level has been estimated for each run, by bandpass filtering in the signal band all pings that did not contain targets, and by selecting the range interval where the background level was independent of range

$$NL = -S_h - G + 10\log[\frac{1}{n}\sum_{i=1}^{n}(\frac{1}{10^{-3}}\int_{t_0}^{t_0+10^{-3}} v_{noise_i}^2 dt)] \tag{8}$$

Where t_0 is an arbitrary starting point for the noise window which was selected to be 1 ms long. The number of pings used on average was 100. In the conditions of the experiment the sonar was noise limited at ranges grater than 150 m.

3.1.7 Background Level (BG)

The Background Level *BG* is defined for each run and each range as the greatest of *NL* and *RL(r)*

$$BG(r) = Max(RL(r), NL) \tag{9}$$

In reverberation limited condition *BG(r)=RL(r),* while in noise limited conditions *BG(r)=NL*

3.1.8 Signal to Background Ratio (SBR)

The Signal to Background Ratio *SBR* for each target, is defined as the difference in decibels between the target echo *EL* and the average background level measured at the target range *BG(R)*:

$$SBR = EL - BG(R) \tag{10}$$

3.1.9 Signal to Reverberation Ratio (SRR)

The Signal to Reverberation Ratio *SRR* for each target, is defined as the difference in decibels between the target echo *EL* and the average reverberation measured at the target range *RL(R)*:

$$SRR = EL - RL(R) \tag{11}$$

In reverberation limited condition *SBR=SRR*

3.1.10 Signal to Noise Ratio (SNR)

The Signal to Noise Ratio for each target is defined as the difference in decibels between the target echo *EL* and the average noise level *NL* for that run.

$$SNR = EL - NL \tag{12}$$

In noise limited conditions *SBR=SNR*

3.1.11 Source Level (SL)

The Source Level SL is the sound pressure level in dB re 1μPa of the transmitted pulse along the axis of the transmit beam pattern, referenced to 1m. Table 3 summarizes the SL for the pulses used during the experiment

Pulse Type	SL Low Freq	SL High Freq
Ricker 4	205.5	235.4
Ricker 6	206.2	235.0
Ricker 8	203.9	234.1
LFM, 2 to 10 KHz, 10 ms	208.5	239.0

Table 3 : Source Level of transmitted signals at primary and secondary frequencies

3.1.12 Target Strength (TS)

The Target Strength TS of each target is derived from the sonar equation as follows

$$TS = EL_{cor} + 2 \times TL - SL \tag{13}$$

3.1.13 Detection Threshold (DT)

The Detection Threshold *DT* is the threshold at the output of the sonar processor necessary to achieve the desired Probability of False Alarm P_{fa}

3.1.14 Signal Excess (SE)

For each target, the Signal Excess *SE* is defined as the difference between the Echo Level, and the Background Level measured at the target range *R*, increased by the Detection Threshold *DT*

$$SE = EL - (BG(R) + DT) \tag{14}$$

3.1.15 *Processing Gain (PG)*

The Processing Gain PG of the sonar receiver is defined as the difference in decibels between the Signal to Background Ratio at the output and the Signal to Background Ratio at the input.

$$PG = SBR_{out} - SBR_{in} \tag{15}$$

3.2 TOPAS runs in reverberation limited conditions

During the experiment, R/V *Alliance* performed several runs over the target fields described in para 2.3. The parametric sonar transmitted various Ricker and LFM pulses, and both the primary (high) and secondary (low) frequency backscattered data were recorded. The HF echoes were received by the TOPAS directional hydrophone, and the LF echoes by the analog broadside beamformer described in para 2.1.2.

At ranges of up to approximately 150 m, the sonar was reverberation limited, and only Ricker pulses were used. At longer ranges the system was noise limited, and only LFM pulses were used. These runs are described in the next paragraph. The HF and LF beam outputs were digitized, bandpass filtered in the signal band, envelope detected and displayed. All relevant parameters of the sonar equation have been measured according to the definitions of para 3.1. Unfortunately, the calibration of the TOPAS receiving chain was not properly logged and therefore the results are presented only in relative terms. Figure 12 shows a typical sonar display of the same target for both high and low frequency. The target tracks are evident as well as the reverberation from the sea floor.

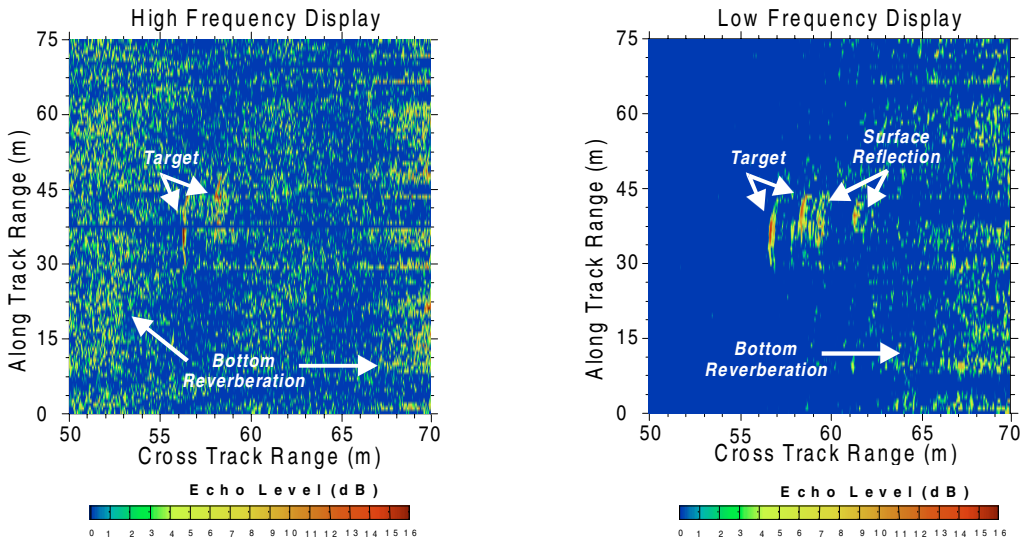

Figure 12 : HF and LF display (run 960601092430, Cyl1) showing detection of the same target at primary and secondary sonar frequencies. Nulls of the HF transmission beampattern are visible in the HF display.

At LF the target track is followed by the surface reflection as the 16 element linear array does not have directivity in the vertical plane; at HF the surface return is attenuated by the directivity of the TOPAS hydrophone. Bottom reverberation is present on both displays, but is more pronounced at HF. For the same run, Figure 13 shows the echo levels of all targets detected at HF and LF and the average reverberation level.

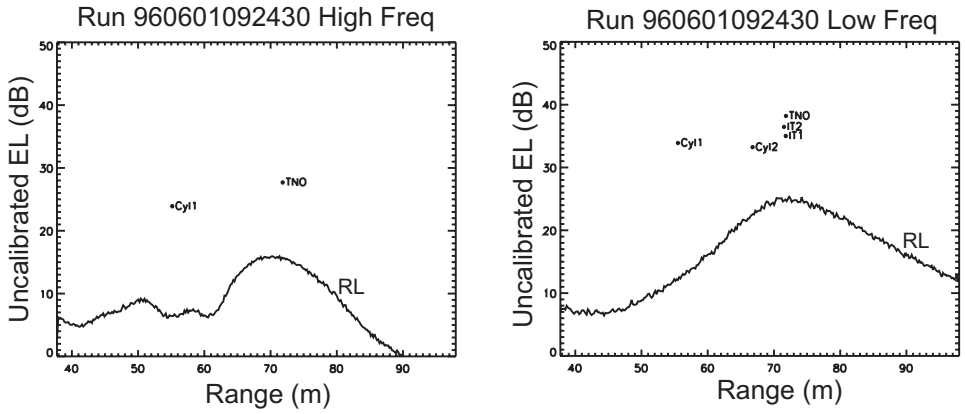

Figure 13 : HF and LF Reverberation and Echo Levels for run 960601092430. The levels are not calibrated and the two figures can not be directly compared.

It is interesting to note that three of the targets detected at LF (Cyl2, IT1and IT2) have not been detected at HF: this could be due to the higher reverberation at HF, but also to the fact that the transmit beam at HF is narrower than that at LF and has deep nulls close to the main peak, instead of the symmetrical degradation of the LF beam. It is therefore possible that the targets were not sufficiently insonified by the HF beam. This behaviour was consistently observed during all runs, and the LF signals achieved better detection than the HF.

Table 4 summarizes the results of all runs across the mine field described in para 2.3. The table shows the run order number, the run name, the transmission frequency used , the type of target detected, the ship heading during the run, the target range and grazing angle, and the signal to background ratio measured at the output of the receiver. All runs were reverberation limited. A detection threshold of 10 dB was used.

Run #	Run name	H/L	Target	Heading (deg)	Pulse type	R (m)	θ (deg)	SBR (dB)
1	960531080457	HF not available						
1	960531080457	LF	Cyl1	158	RK 6	69.2	19.8	13.4
1	960531080457	LF	Cyl2	158	RK 6	77.6	17.6	10.9
1	960531080457	LF	IT2	158	RK 6	66.2	20.8	14.6
1	960531080457	LF	TNO	158	RK 6	80.2	17.0	10.9
2	960531152806	HF	Cyl1	160	RK 6	55.2	25.2	20.9
2	960531152806	HF	Cyl2	160	RK 6	55.5	25.0	14.5
2	960531152806	HF	TNO	160	RK 6	62.5	22.1	20.2
2	960531152806	LF	Cyl1	160	RK 6	55.4	25.1	24.5
2	960531152806	LF	IT1	160	RK 6	56.3	24.7	12.4
2	960531152806	LF	IT2	160	RK 6	42.0	34.0	22.1
2	960531152806	LF	TNO	160	RK 6	64.9	21.2	18.2
3	960601082100	HF	Cyl1	156	RK 8	66.1	20.8	23.0
3	960601082100	HF	IT2	156	RK 8	60.7	22.8	12.3
3	960601082100	HF	TNO	156	RK 8	65.0	21.2	14.1
3	960601082100	LF	Cyl1	157	RK 8	66.3	20.8	16.9
3	960601082100	LF	Cyl2	157	RK 8	61.9	22.3	14.7
3	960601082100	LF	IT1	157	RK 8	78.4	17.4	10.2
3	960601082100	LF	IT2	157	RK 8	61.0	22.7	24.4
3	960601082100	LF	TNO	157	RK 8	65.4	21.1	15.3
4	960601085230	HF	Cyl1	334	RK 8	88.5	15.4	15.6
4	960601085230	HF	TNO	334	RK 8	79.2	17.3	10.3
4	960601085230	LF	Cyl2	334	RK 8	72.0	19.1	12.8
4	960601085230	LF	IT1	334	RK 8	78.2	17.5	10.9
4	960601085230	LF	IT2	334	RK 8	75.5	18.1	10.1
4	960601085230	LF	TNO	334	RK 8	79.7	17.1	13.3
5	960601092430	HF	Cyl1	158	RK 8	54.8	25.4	16.8
5	960601092430	HF	TNO	158	RK 8	71.5	19.2	11.8
5	960601092430	LF	Cyl1	158	RK 8	55.1	25.2	21.4
5	960601092430	LF	Cyl2	158	RK 8	66.4	20.7	10.5
5	960601092430	LF	IT1	158	RK 8	71.4	19.2	9.9
5	960601092430	LF	IT2	158	RK 8	71.1	19.3	10.9
5	960601092430	LF	TNO	158	RK 8	71.4	19.2	13.0
7	960601110130	HF	Cyl1	326	RK 4	73.6	18.6	12.5
7	960601110130	HF	Cyl2	326	RK 4	72.0	19.0	10.1
7	960601110130	HF	TNO	326	RK 4	48.4	29.0	11.9
7	960601110130	LF	Cyl1	326	RK 4	74.2	18.5	11.1
7	960601110130	LF	IT2	326	RK 4	70.1	19.6	12.3
7	960601110130	LF	TNO	326	RK 4	51.0	27.4	12.8
8	960601132459	HF	Cyl1	337	RK 6	79.9	17.1	12.3
8	960601132459	HF	TNO	337	RK 6	70.8	19.4	11.4
8	960601132459	LF	Cyl1	336	RK 6	82.1	16.6	17.7
8	960601132459	LF	Cyl2	336	RK 6	81.4	16.8	9.7
8	960601132459	LF	IT1	336	RK 6	70.3	19.5	13.5
8	960601132459	LF	IT2	336	RK 6	79.5	17.2	17.2
8	960601132459	LF	TNO	336	RK 6	71.1	19.3	15.2

Table 4: Summary of TOPAS runs against mine field

Table 5 summarizes the results of all runs against the cluster of mines described in para 2.3. All runs, except the last two, were clearly reverberation limited. The last two were in a transition region where both noise and reverberation contributed to the background.

Run #	Run name	H/L	Target	Heading (deg)	Pulse type	R (m)	θ (deg)	SBR (dB)
9	960602140008	HF	Cluster	166	RK 8	67.1	20.5	15.4
9	960602140008	LF	Cluster	167	RK 8	67.4	20.4	20.0
10	960602142438	HF	Cluster	180	RK 8	71.9	19.1	11.8
10	960602142438	LF	Cluster	180	RK 8	73.0	18.8	15.3
11	960602144647	HF	Cluster	143	RK 8	56.0	24.8	16.4
11	960602144647	LF	Cluster	168	RK 8	56.1	24.8	21.2
12	960602152004	HF	Cluster	270	RK 8	79.2	17.3	10.2
12	960602152004	LF	Cluster	270	RK 8	79.2	17.3	11.5
13	960602160746	HF	Cluster	278	RK 8	65.1	21.2	17.0
13	960602160746	LF	Cluster	278	RK 8	66.4	20.7	20.2
14	960602162859	HF	Cluster	90	RK 8	38.9	37.2	25.9
14	960602162859	LF	Cluster	90	RK 8	39.5	36.5	14.7
15	960602165400	HF	Cluster	220	RK 8	71.0	19.3	15.2
15	960602165400	LF	Cluster	216	RK 8	71.7	19.1	12.9
16	960602175640	HF	Cluster	140	RK 8	68.0	20.2	11.7
16	960602175640	LF	Cluster	141	RK 8	68.1	20.2	13.3
17	960602185613	HF	Cluster	180	RK 8	150.8	9.0	13.1
17	960602185613	LF	Cluster	180	RK 8	152.0	8.9	18.7
18	960602192742	HF	Cluster	20	RK 8	147.9	9.1	21.4
18	960602192742	LF	Cluster	12	RK 8	148.9	9.1	18.5

Table 5 : Summary of TOPAS runs against the cluster of mines

The LF mode of operation achieved 30 detections against the mine field and 10 detections against the cluster. The HF mode had only 15 detections against the mine field, and 10 detections against the cluster. If we compare the SBR for all targets detected by both HF and LF, the LF outperforms the HF by approximately 2 dB. Figure 14 shows the signal to background ratio for all targets: although the TS of the targets should theoretically increase by approximately 6 dB at broadside from LF to HF [8, page 274], the SBR is on average about 2 dB higher at low frequency.

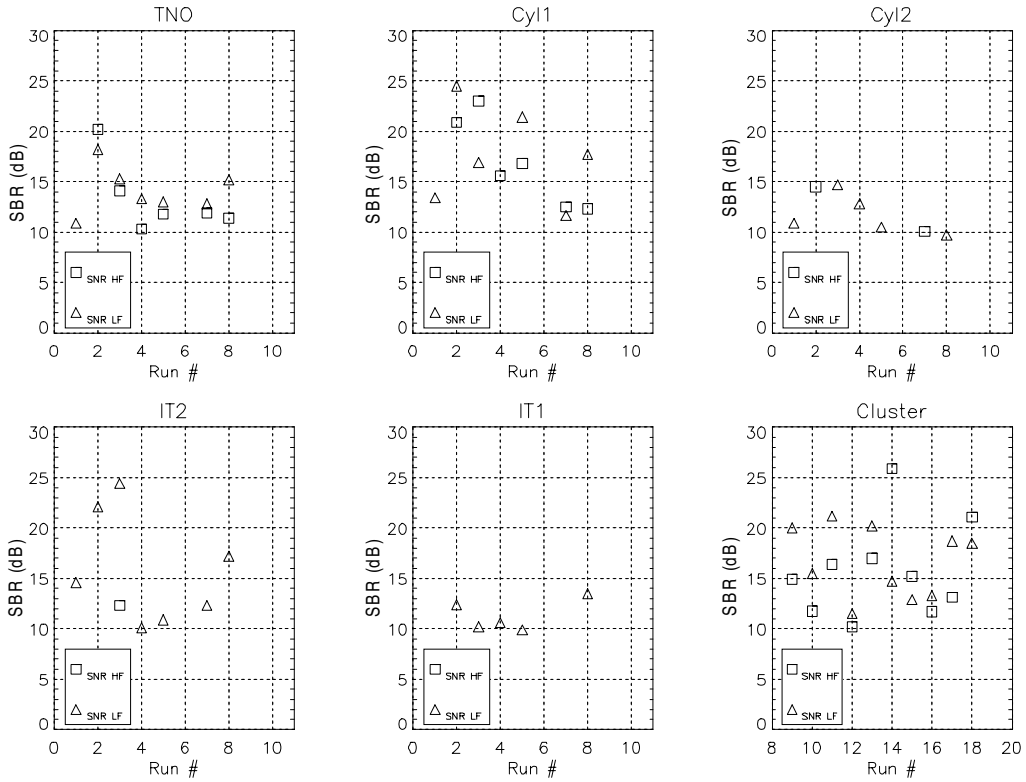

Figure 14 : Signal to Background Ratio of six different targets for all TOPAS runs in reverberation limited conditions

3.3 TOPAS runs in noise limited conditions

During the experiment, a few runs were conducted to test the performance of the sonar at long range and very low grazing angles (below 5 degrees) against the cluster of mines. As it was expected that the sonar would be noise limited, the energy of the transmitted pulses was maximized, and a Linear Frequency Modulated (LFM) pulse of 10 ms with bandwidth from 2 to 10 kHz was used. The target echoes were received by the analog beamformer described in para 2.1.2, bandpass filtered in the signal band, and cross correlated with a synthetic replica of the transmitted signal. Figure 15 shows the display of the four runs. The tracks of the three mines of the cluster are clearly visible in all runs. The asymmetry of the echo strength relative to the point of closest approach is probably due to the change in orientation of the targets.

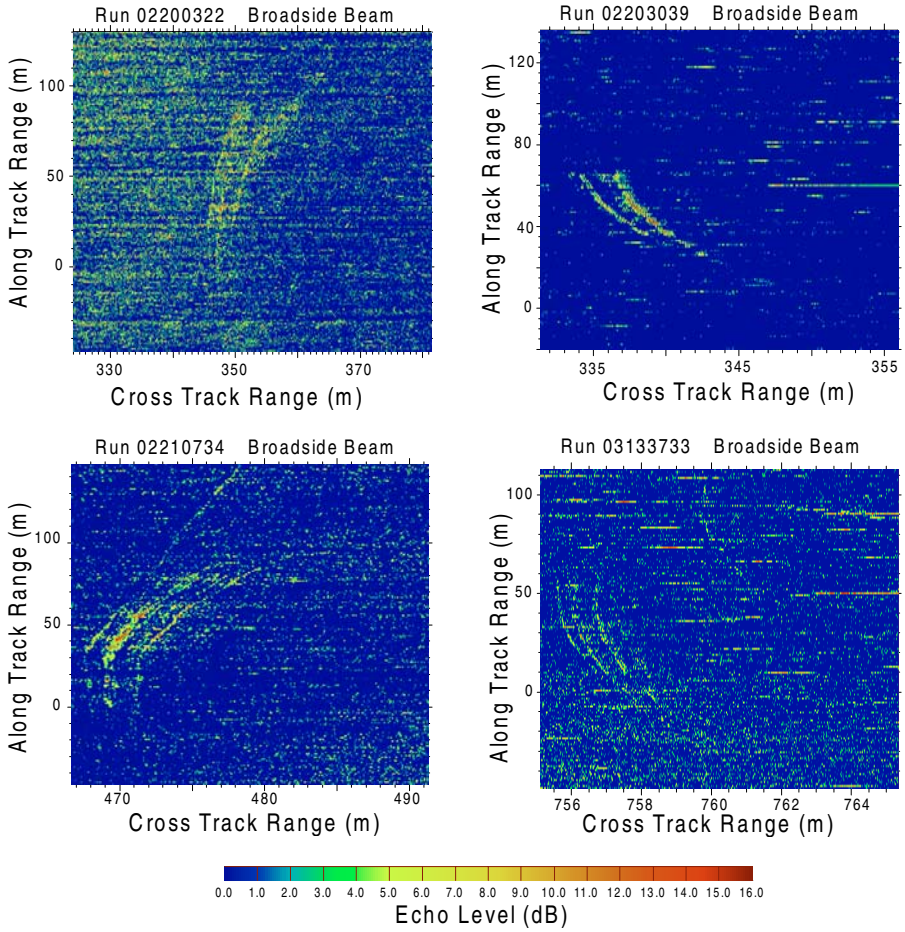

Figure 15 : Displays of four long range TOPAS runs

The performance of the sonar is characterized by the signal to noise ratio at the output of the receiver measured as follows

$$SNR_{out} = 10\log(S_{peak}^2) - NL_{out} \tag{16}$$

Where S_{peak} is the peak of the cross correlator output for a given target, and NL_{out} is the noise power at the output of the processor. The processing gain PG of such a receiver is usually defined as the difference in dB between the output and input signal to noise ratios. The cross correlator used to analyze the data, is calibrated in such a way that an LFM with 1 V_{rms} amplitude generates a peak of 1 V at the processor output. The processing gain can therefore be estimated by subtracting the output noise level from the input noise level

$$PG = NL_{in} - NL_{out} \tag{17}$$

The theoretical *PG* is 10log(*2BT*), where *BT* is the time bandwidth product, and is equal to 22 dB for the LFM used. This is achieved against white noise and with a replica that correlates perfectly with the transmitted signal. In our case, the transmitted signal is not a perfect LFM (see Figure 4), and a slight loss occurs when it correlates with a synthetic replica (about 1.5 dB loss). Moreover, at short range the sonar is not clearly noise limited and a combination of noise and reverberation contributes to the background level. For these two reasons, the processing gain achieved is lower than predicted by theory. When the target range increases, the noise dominates and the processing gain obtained is closer to the theoretical value. Table 6 shows the summary of the four TOPAS runs at long range

Run name	Target	Pulse type	R (m)	θ (deg)	SNR_{out} (dB)	Proc Gain (dB)
LF960602200322	Cluster	FM 2-10 KHz, 10 ms	349.2	3.9	18.3	14.5
LF960602203039	Cluster	FM 2-10 KHz, 10 ms	338.9	4.0	23.1	16.5
LF960602210734	Cluster	FM 2-10 KHz, 10 ms	471.3	2.9	20.3	17.0
LF960603133733	Cluster	FM 2-10 KHz, 10 ms	756.0	1.8	15.0	19.0

Table 6 : Summary of four long range TOPAS runs

Figure 16 shows the measured output echo and noise levels, and the measured input noise level.

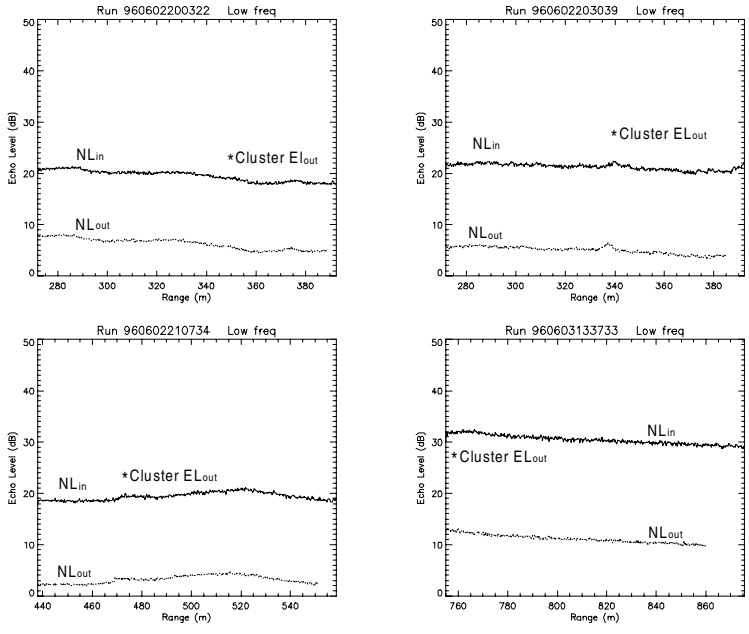

Figure 16 : Output Echo Level and Input and Output Noise Levels for long range TOPAS runs

3.4 ADAM runs

For a few runs all hydrophone signals of the receiving array were acquired by the ADAM acquisition system described in para 2.1.2. As the calibration of the ADAM system is known, it is possible to present the results of these runs in absolute levels. The hydrophone signals were digitized, filtered in the band of the secondary frequency and beamformed to form a few beams covering the area insonified. The TOPAS beam outputs were envelope detected and displayed. Figure 17 shows a typical display of seven beams around broadside, with cross track range along the vertical axis and along track range from left to right on the horizontal axis of each beam. Target tracks appearing first on the forward looking beams (0 is the forward endfire, 180 is the rear endfire), have their maximum in the broadside beam, and continue in the rear looking beams.

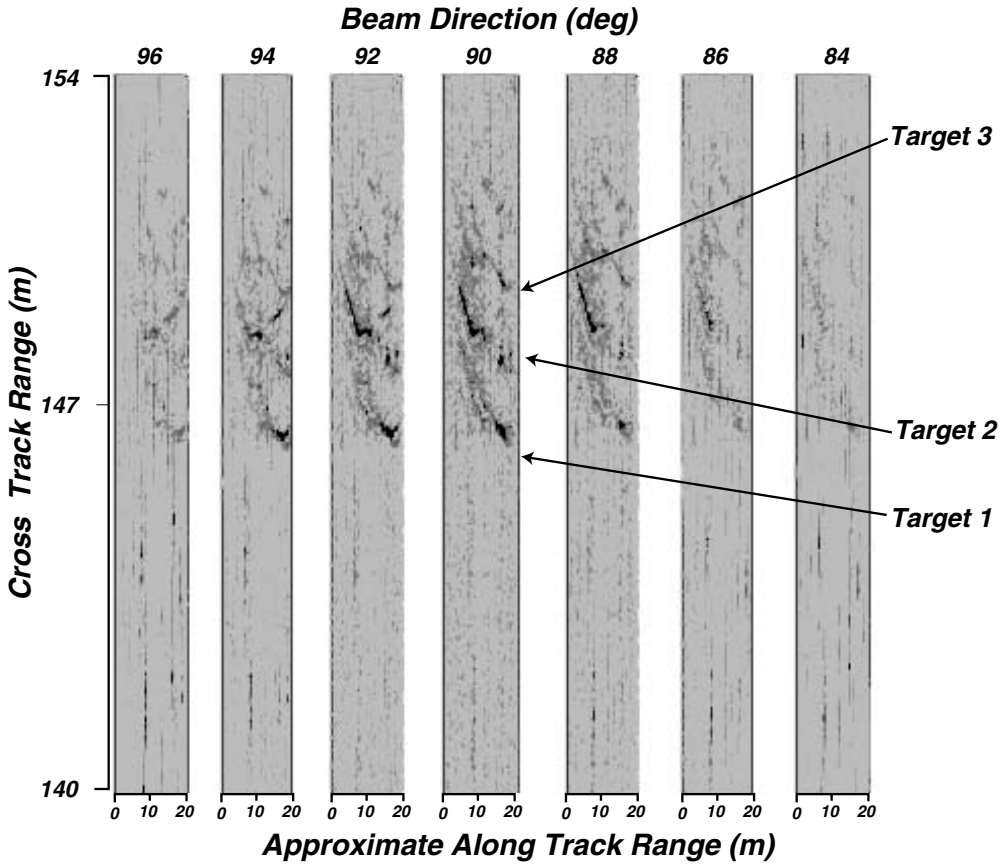

Figure 17 : Multi beam display for Run 02202858 at secondary frequency

As the maximum target response has always been found in the broadside beam, only this beam has been utilized in the analysis of the ADAM runs. Figure 18 shows the waterfall display of the raw broadside beam for the same run: as in the previous display the parabolic tracks of the three targets of the mine cluster are clearly visible

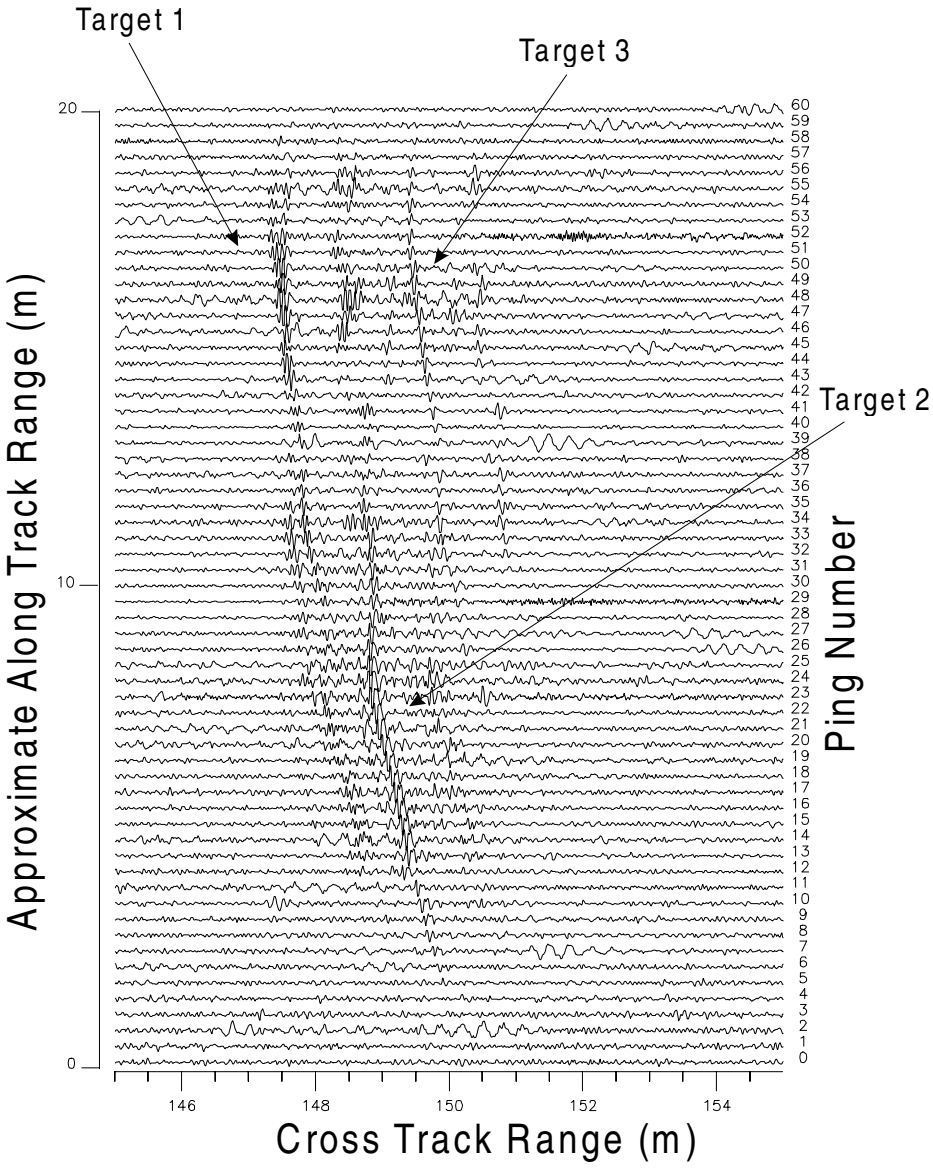

Figure 18 : Waterfall Display of Broadside Beam for run 960602202858 at secondary frequency.

Table 7 summarizes the results of all ADAM runs against the mine field and the cluster described in para 2.3. The table shows the run name, the type of target detected, the ship heading during the run, the pulse type used, the target range and grazing angle, the measured target echo level, the average reverberation level measured at the target range, the beampattern correction applied to the target echo and to the reverberation, their corrected levels, the source level of the transmitted pulse, the propagation loss at the target range (assuming spherical spreading), the computed target strength and the signal to background ratio measured at the output of the digital beamformer.

Run name	Target	Heading (deg)	Pulse Type	R (m)	θ (deg)	EL (dB)	RL (dB)	BP_{corr} (dB)	EL_{corr} (dB)	RL_{corr} (dB)	SL (dB)	TL (dB)	TS (dB)	SBR (dB)
960601095032	TNO	334	RK 8	79.5	17.2	107.1	92.8	2.6	109.7	95.4	204.0	76.0	-18.3	14.3
960601095032	IT2	334	RK 8	93.5	14.6	104.3	85.1	9.0	113.3	94.1	204.0	78.8	-11.9	19.2
960601102815	Cyl1	158	RK 8	54.9	25.4	103.1	82.0	14.2	117.3	96.2	204.0	69.6	-17.1	21.1
960601102815	Cyl2	158	RK 8	68.8	20.0	102.8	94.8	0.0	102.8	94.8	204.0	73.5	-27.6	8.0
960601102815	TNO	158	RK 8	71.2	19.3	110.7	96.1	0.7	111.4	96.8	204.0	74.1	-18.5	14.6
960602145808	Cluster	166	RK 8	67.2	20.5	112.1	89.1	2.2	114.3	91.3	204.0	73.1	-16.6	23.0
960602152311	Cluster	180	RK 8	72.6	18.9	112.9	93.2	0.1	113.0	93.3	204.0	74.4	-16.6	19.7
960602154517	Cluster	168	RK 8	55.8	24.9	101.3	81.5	14.6	115.9	96.1	204.0	69.9	-18.3	19.8
960602161830	Cluster	270	RK 8	82.9	16.5	103.2	92.3	3.9	107.1	96.2	204.0	76.7	-20.1	10.9
960602170605	Cluster	278	RK 8	66.1	20.8	108.8	88.5	6.1	114.9	94.6	204.0	72.8	-16.3	20.3
960602175444	Cluster	220	RK 8	71.4	19.2	108.4	94.3	0.3	108.7	94.6	204.0	74.2	-21.2	14.1
960602185730	Cluster	140	RK 8	67.8	20.3	110.7	96.2	0.3	111.0	96.5	204.0	73.2	-19.8	14.5
960602202807	Cluster	12	RK 8	148.6	9.1	107.5	86.5	0.4	107.9	86.9	204.0	86.9	-9.2	21.0

Table 7 : Summary of ADAM runs

The median value of the measured target strength is −17.8 dB and therefore a value of −18dB has been used in the modelling, as representative of the conditions of the experiment. Figure 19 shows the targets *EL* and the average reverberation for all ADAM runs. All are clearly reverberation limited except the last.

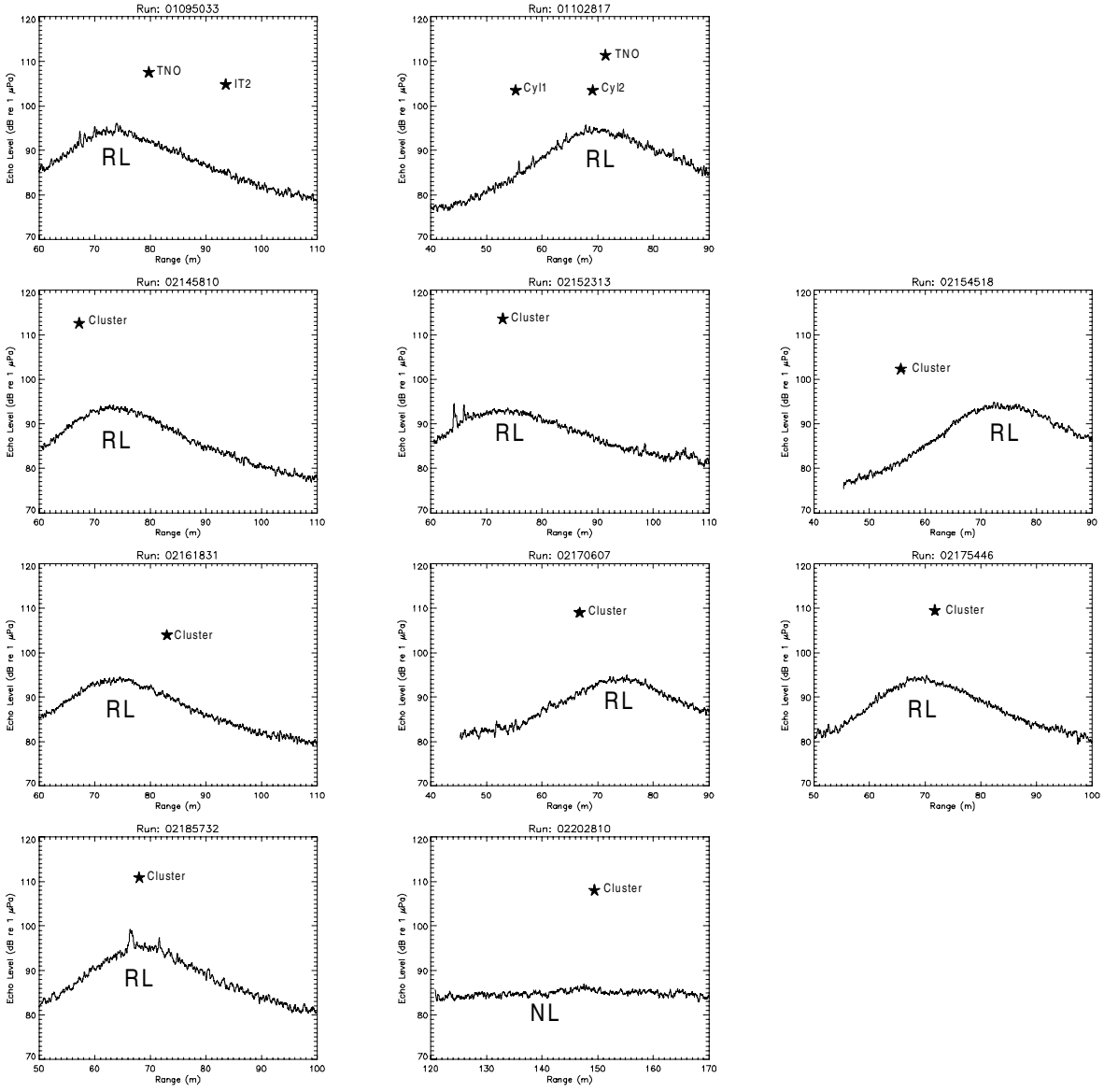

Figure 19 : Echo Level and Background Level for all targets of ADAM runs

4
Sonar equations

In this section we compare the sonar parameters measured in the ADAM runs with a simple model of the sonar equation based on Lambert's approximation for bottom backscattering [8, page 250]. Lambert's law assumes that the backscattered power is proportional to the square of the sine of the grazing angle.

$$S_s = 10\log\mu + 10\log(\sin^2\theta) \tag{18}$$

Where S_s is the backscattering coefficient, $10\log\mu$ is a proportionality constant, named Lambert's coefficient, which depends on the bottom type, and θ is the grazing angle. This is only a crude approximation of the complex physical processes involved in backscattering from the sea floor, but is useful for a first look at the performance of the sonar system used during the experiments. To model the case of buried targets, we make the following assumptions:

1. Targets re-radiate in the direction of the transmitted pulse

2. Targets in the sediment have the same TS as in water

If this is true, we can model the buried targets by adding to the transmission loss an extra loss, which is due to the propagation of the transmitted pulse into the sediment. These conditions are unlikely to be satisfied in practice, and in general it is expected that they are over optimistic. In particular, for angles below the critical angle, little energy penetrates the sediment, and furthermore the target reradiates predominantly in the vertical and not in the backscattering direction [9]. However it is interesting to consider this simple model as it represents an upper bound to the performance of the sonar against buried targets.

In the next sections we model the reverberation level and the echo of a -18 dB target, we compute the signal excess for the proud target case, and we compare the model with the measured data. We model the case of a buried target assuming two values of the propagation loss into the sediment, and we see how this causes sonar performance to deteriorate. We also model the TOPAS runs when the LFM pulses have been used to achieve long range detection in a noise limited environment, and we compare with the measured data. Finally, we predict the performance of the sonar when a longer receiving array will replace the 16 element array used during the experiment.

4.1 Reverberation Level

The variation of the reverberation level with range r is given by

$$RL(r) = SL - 2 \times TL + S_s + 10 \log A \tag{19}$$

Where SL is the transmitter Source Level, TL is the one way transmission loss at range r, S_s is the backscattering coefficient, and A is the bottom area that contributes to the reverberation. The area A can be approximated [8, page 219] as a function of the transmit-receive -6dB beamwidth Φ, the range r, and the transmitted pulsewidth τ

$$A = r \times \Phi \times \tau \times c / 2 \tag{20}$$

For the ADAM runs, the cross range resolution is 0.25 ms and the transmit-receive –6dB beamwidth is approximately 6° as shown in Figure 20 (the receive beam pattern is computed for a frequency of 8 kHz). However, the –6 dB boxcar approximation does not take into account the triangular shape of the TOPAS low frequency transmit beam pattern. The figure shows also the correct boxcar approximation to the transmit-receive beamwidth (computed by numerical integration of the transmit and receive beam patterns) and indicates that a value of 8° is more appropriate

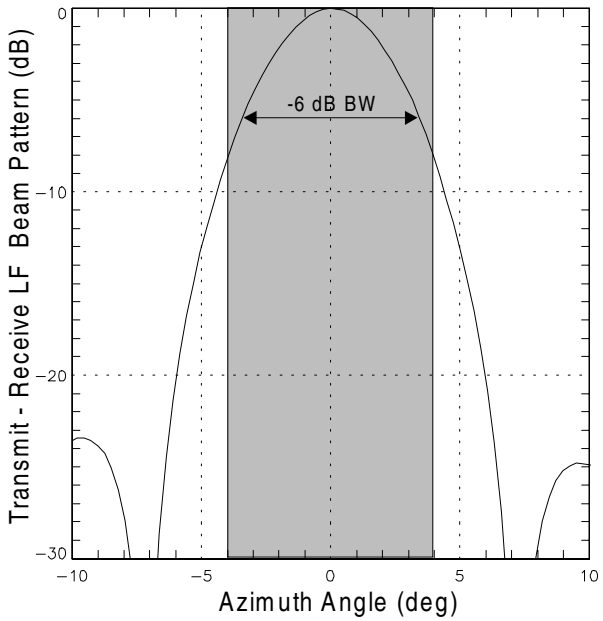

Figure 20 : Transmit-Receive Azimuth Beam Pattern at 8kHz

The reverberation level becomes

$$RL(r) = SL - 2 \times TL + S_s + 10\log(r \times \Phi \times \tau \times c/2) \tag{21}$$

Therefore, combining equations (18), (19) and (20) and assuming spherical spreading, we have

$$RL = SL - 40\log r + 10\log \mu + 10\log \sin^2(\theta) + 10\log(r \times \Phi \times \tau \times c/2) \tag{22}$$

At low grazing angles, $\sin^2(\theta)$ can be approximated by $(h/r)^2$ where h is the sonar distance from the sea floor.

4.2 Echo Level

Under the assumption of spherical spreading, the variation with range r of the echo level of a proud target the target strength of which TS, is given by

$$EL_{proud}(r) = SL - 40\log r + TS \tag{23}$$

Following the two assumptions in paragraph 4, the echo level of a buried target will depend on the propagation loss into the sediment. If we call the one way propagation loss into the sediment Sediment Loss ($SedL$), we will have

$$EL_{buried}(r) = SL - 40\log r + TS - 2 \times SedL \tag{24}$$

4.3 Signal Excess

Following the definition of signal excess of para 3.1.14 and combining it with (21) and (24), in reverberation limited environment we have

$$\begin{aligned} &SE = EL - (RL + DT) = \\ &(SL - 40\log r + TS - 2 \times SedL) - \\ &(SL - 40\log r + 10\log \mu + 10\log \sin^2(\theta) + 10\log(r \times \Phi \times \tau \times c/2) + DT) = \\ &TS - 2 \times SedL - (10\log \mu + 10\log \sin^2(\theta) + 10\log(r \times \Phi \times \tau \times c/2) + DT) \end{aligned} \tag{25}$$

In noise limited conditions we have

$$SE = (SL - 40\log r + TS - 2 \times SedL) - (NL + DT) \tag{26}$$

A value of 10 dB for the Detection Threshold is typical of many sonar cases. In noise limited conditions, it is convenient to increase the energy of the transmitted signal, and

often linear frequency modulated (LFM) pulses are used: in this case, the signal excess is increased by the processing gain achieved.

$$SE = (SL - 40\log r + TS - 2 \times SedL) - (NL + DT) + 10\log(2 \times B \times T) \quad (27)$$

4.4 Discussion

The parameters used to model the experimental data are listed in the table 8

Parameter	Symbol	Unit	Value
Source Level			
8 KHz Ricker	*SL*	dB re 1µPa @ 1m	204
LFM 2-10KHz, 10 ms	*SL*	dB re 1µPa @ 1m	208.5
Tx-Rx Equivalent Beamwidth	ϕ	deg	8
Cross range integration window			
8 KHz Ricker	τ	ms	0.25
LFM 2-10KHz, 10 ms	τ	ms	0.25
Sonar depth over the bottom	h	m	23.5
Lambert coefficient	10 log (μ)	dB re 1µPa / m^2	-29
Noise Level	*NL*	dB re 1µPa	82
One way transmission loss	*TL*	dB	20 log (r)
One way transmission loss in sediment	*SedL*	dB	0 - 5 - 10
Detection threshold	*DT*	dB	10
Target Strength	*TS*	dB	-18

Table 8 : Parameters used for the modelling

For transmission loss we have assumed spherical spreading and disregarded volume absorption loss which is negligible at the frequency of interest. For transmission loss in the sediment we have examined three values, 0 (i.e. the proud target case), 5 and 10 dB. Figure 21 compares the modelled echo and reverberation with the measured data. As explained in para 3.1, the measured echo and reverberation have been corrected to compensate for the beampattern effects of the sonar.

The modelled echo level falls less rapidly with range than the modelled reverberation because EL is proportional to R^{-4} (see equation 23) while RL is proportional to R^{-5} (see equation 22).

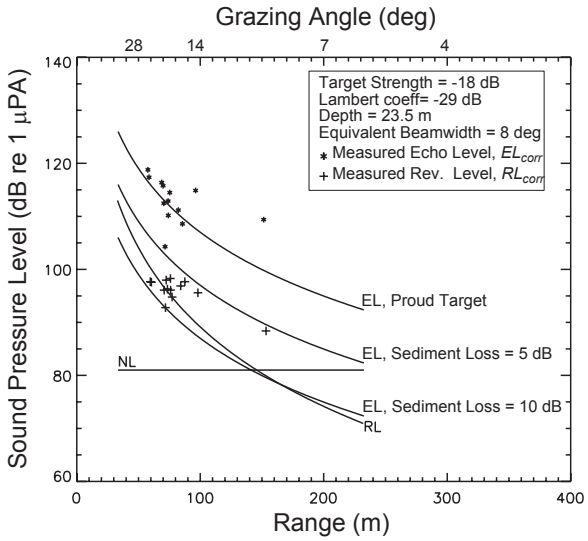

Figure 21 : Modelled and measured EL and RL for the 16 element array

There is in general good agreement between modelled and measured target echo levels, while measured reverberation is higher than that predicted by Lambert's law as it falls like R^{-4}. The figure shows that even assuming moderate absorption of sound propagating into the sediment (5 dB one way), the target echo level will be masked by reverberation. Figure 22 compares the modelled and measured signal excess for all ADAM runs. A -18 dB buried target would be detected by the sonar used in this experiment, only if the sediment attenuates the incoming pulse by less than 2 dB (one way).

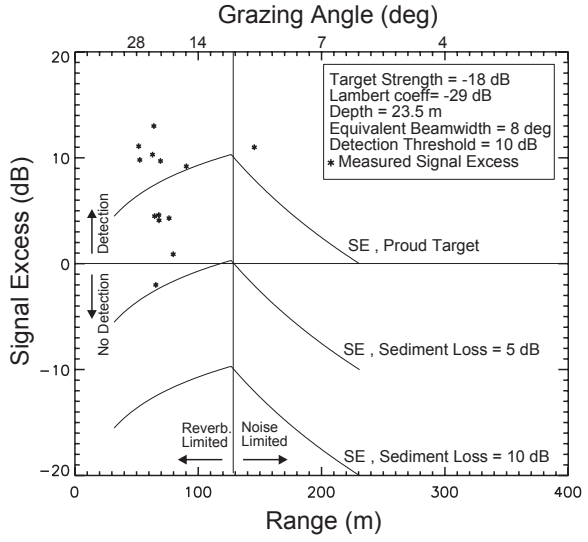

Figure 22 : Modelled and measured Signal Excess for the 16 element array

Figure 23 compares the modelled and measured signal excess for the noise limited case with LFM pulses. According to equation (27) the SE curves are shifted upwards by the processing gain.

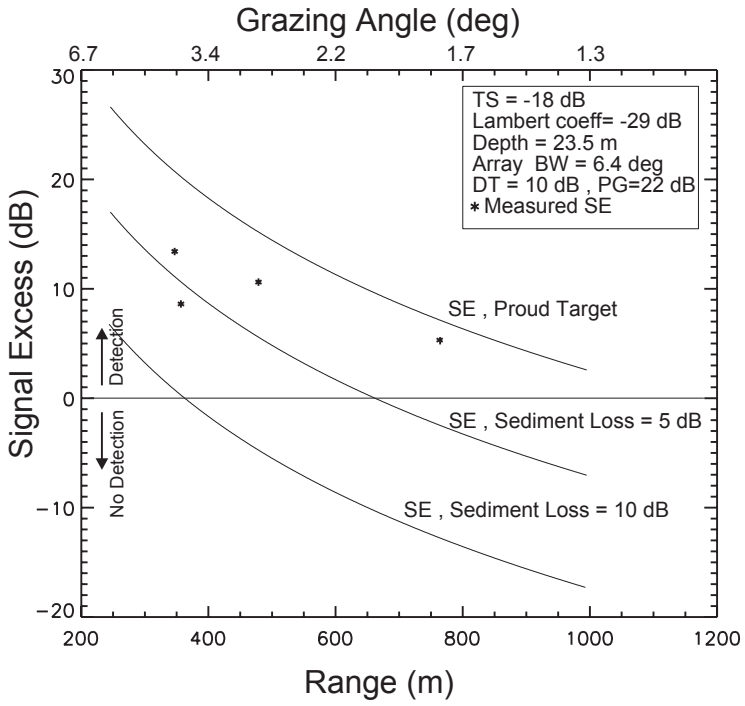

Figure 23 : Modelled and measured Signal Excess for LFM (16 element array)

The signal excess measured at shorter range is less than predicted, and this is due to the fact that not all processing gain has been achieved as discussed in para 3.2

SACLANTCEN has procured a new receiving 128 element array to improve sonar performance. The new array has a beamwidth of 0.8°, and in combination with the TOPAS generates a transmit-receive beampattern with an equivalent beamwidth of 1°. The echo, reverberation and signal excess for the new sonar, modelled for the conditions of the experiment reported in this paper, are shown in Figure 24 and 25 for the 8kHz Ricker transmission.

The effect of the new array is to reduce both the noise and the reverberation by 10log(128/16)=9 dB.

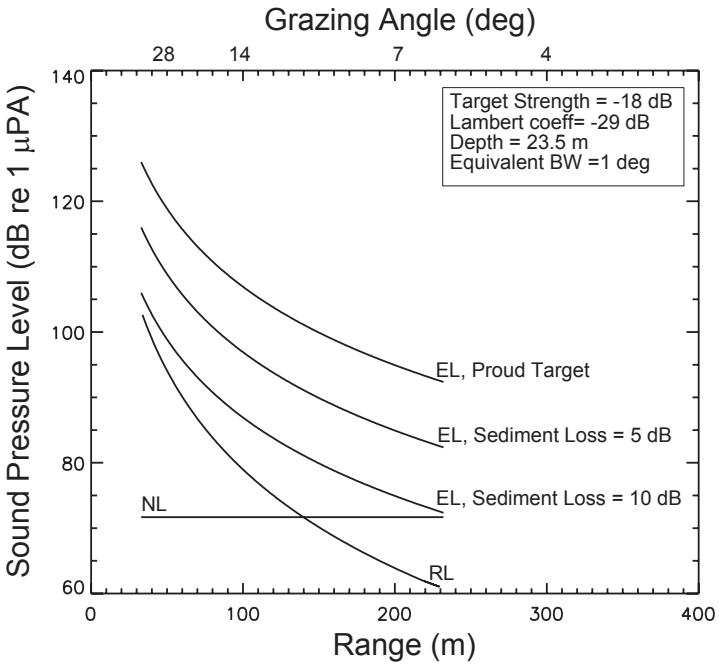

Figure 24 : Modelled EL and RL for the 128 element array

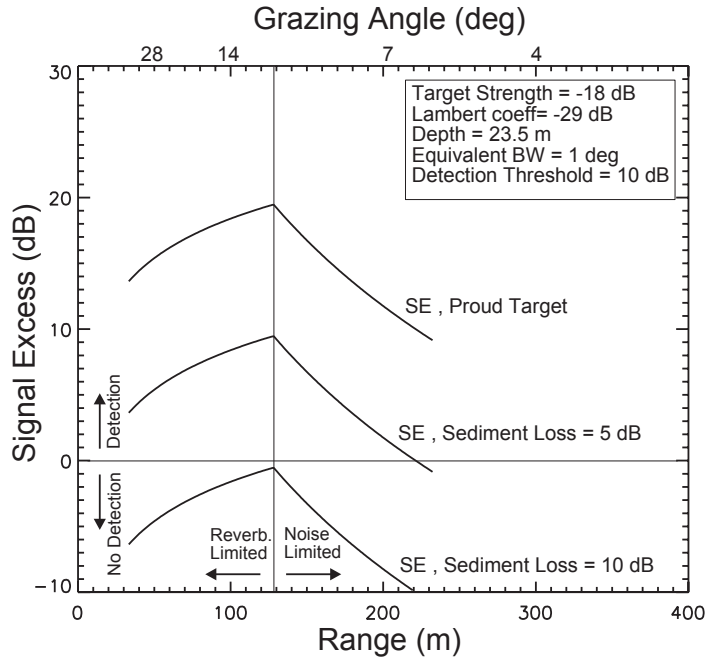

Figure 25 : Modelled Signal Excess for the 128 element array

The simple analysis presented in this paragraph shows that the sonar described in this report is unlikely to detect buried targets if the one way propagation loss in the sediment exceeds 2 dB. The improvement in reception due to the new 128 element array would allow detection of targets buried in sediment with one way transmission loss of the order of 6 or 7 dB (2 dB plus half of the gain due to the new array).

It should be stressed that these figures represent only an upper bound to the sonar performance, as the assumptions stated in paragraph 4 are unlikely to be satisfied in practice, and more unfavorable conditions may be expected. In order to better characterize the performance of a low grazing angle sonar against buried targets, it is important to have a clear understanding of the propagation loss of the transmitted pulses into the sediment, and of the buried target response in the azimuthal and vertical plane.

5
Conclusion and future work

This experiment has demonstrated the feasibility of using the TOPAS parametric transmitter and a linear receiving array, mounted as a side scan sonar, for the detection of proud targets, positioned on a sandy bottom, in shallow water at a depth of 26 m.

Detection of a variety of cylindrical proud targets has been achieved in reverberation and noise limited conditions, up to a range of 750 m, using both the primary (40 kHz) and secondary frequencies (2 to 12 kHz) of the parametric source. For the conditions of the experiment, the noise level measured on the broadside beam of the receiving array exceeded the reverberation at approximately 150 m range. In reverberation, short, broadband, Ricker pulses were used to improve the range resolution of the sonar, while at longer range, 10 ms LFM pulses were transmitted to counter the noise level.

The secondary frequency of the TOPAS achieved better results for two different reasons:

- The bottom backscattering coefficient decreases with frequency more rapidly than the increase with frequency of the target strength. The overall signal excess for a given target is therefore greater at LF than at HF. The LF mode of operation achieved 30 detections against a mine field of six different targets and 10 detections against a cluster of three targets. The HF mode had only 15 detections against the mine field, and 10 detections against the cluster. Comparing the SBR (Signal to Background Ratio) for all targets detected by both HF and LF, the LF outperforms the HF by approximately 2 dB. Although the TS of the targets should theoretically increase from LF to HF, the SBR is in average about 2 dB higher at low frequency.

- The beam of the transmitter at primary frequency is narrower than that at secondary and has deep nulls close to the main peak, instead of the triangular degradation of the secondary beam. It is therefore possible that the targets were not sufficiently insonified by the HF beam. This effect was consistently observed during all runs, and several targets clearly detected at LF were completely absent at HF, probably because they were in the nulls of the HF beam.

The conditions of the experiment were modelled with a simple sonar equation based on Lambert's law. There is in general a good agreement between modelled and measured target echo levels, while the measured reverberation is higher than that predicted by Lambert's law. In order to assess the potential of the proposed configuration against buried targets, a parametric study was performed to assess the amount of extra loss that the sonar could afford when the transmitted pulses propagate into the sediment. The

proposed sonar was unlikely to detect a target of –18 dB[1] buried in sand if the extra transmission loss into the sediment exceeds 2 dB (one way propagation).

This negative result can be partly overcome by a longer receiver to improve horizontal resolution. The effect of the new 128 element array has also been modelled and the upgraded sonar should be capable of achieving detections of a –18 dB target buried in sand, with one way transmission loss of the order of 6 or 7 dB.

It should be stressed that these figures represent only an upper bound to the sonar performance. The assumptions in paragraph 4 are unlikely to be satisfied in practice, and in general more unfavorable conditions may be expected.

In order to better characterize the performance of a low grazing angle sonar against buried targets, it is important to have a clear understanding of the propagation loss of the transmitted pulses into the sediment and of the buried target response in the azimuthal and vertical plane. For this reason, a few experiments have already been planned to measure the frequency response of the sediment as a function of bottom type, transmitted frequency, burial depth and grazing angle. At the same time, the spatial response of the buried targets will be studied, with models and field experiments, over a broad range of frequencies, burial depths and grazing angles.

Future work will include the evaluation at sea of the side scan parametric sonar approach, combined with the new 128 element array for the detection of buried targets. Different ranges (i.e. different grazing angles) from the sonar to the targets will be considered, in order to evaluate the performance of the selected approach for the detection of buried mines, as a function of grazing angles.

[1] The value of –18 dB has been selected for the modelling because it represents the median value of the six targets measured during the experiment. If a stronger target had to be detected, the conclusions reported here would have to be scaled to the new target strength.

References

[1] Pethersen, J. M. Hovem, and A. Lovik, A new sub-bottom profiling sonar using a non-linear sound source, *Radio Elect. Eng*., **47**, 3,. 1977: 105-111.

[2] Chotiros, N. Biot model of sound propagation in water-saturated sand, *Journal of the Acoustical Society of Am*erica, **97**, 1995: 199-234.

[3] Thorsos, E.I., Jackson, D.R., Moe, J.E., Williams, K.L., *Modeling of subcritical penetration into sediments due to interface roughness*, Proceedings of the conference on High-frequency Acoustics in shallow water. Lerici, July 1997.

[4] Jensen, F.B., Schmidt, H. *Subcritical penetration of narow gaussian beams into sediment*, SACLANTCEN SR-134, La Spezia, Italy, NATO SACLANT Undersea Research Centre, 1988.

[5] Stephen, R.A., Bolmer, S.T. The direct wave root in Marine seismology, *Bulletin of the seismological society of America*, **75**, 1, 1985: 57-67.

[6] Maguer, A., Bovio, E., Fox, W. Sound penetration into a sandy bottom below and above critical angle, SACLANTCEN report in preparation.

[7] Bergem, O., Pace, N.G. Calibration of the TOPAS PS040. Part I: Measurements recorded with TOPAS acquisition system, SACLANTCEN M-119, La Spezia, Italy, NATO SACLANT Undersea Research Centre, 1996.

[8] Urick, R.J., Principles of underwater sound, *McGraw Hill*, 1975.

[9] Hovem, J., SACLANTCEN report in preparation

Report no. changed (Mar 2006): SM-346-UU

NATO Undersea Research Centre
Viale San Bartolomeo 400
19138 La Spezia, Italy